A transient based protection technique for future DC grids utilising travelling wave power

Ikhide, M., Tennakoon, S., Griffiths, A., Ha, H., Adamczyk, A. & Subramanian, S.

Published PDF deposited in Coventry University's Repository

Original citation:
Ikhide, M, Tennakoon, S, Griffiths, A, Ha, H, Adamczyk, A & Subramanian, S 2018, 'A transient based protection technique for future DC grids utilising travelling wave power' IET Journal of Engineering, vol. 2018, no. 15, pp. 1267-1273.
https://dx.doi.org/10.1049/joe.2018.0186

DOI 10.1049/joe.2018.0186
ESSN 2051-3305

Publisher: IET

This is an open access article published by the IET under the Creative Commons Attribution License (http://creativecommons.org/licenses/by/3.0/)

Copyright © and Moral Rights are retained by the author(s) and/ or other copyright owners. A copy can be downloaded for personal non-commercial research or study, without prior permission or charge. This item cannot be reproduced or quoted extensively from without first obtaining permission in writing from the copyright holder(s). The content must not be changed in any way or sold commercially in any format or medium without the formal permission of the copyright holders.

The Journal of Engineering

The 14th International Conference on Developments in Power System Protection (DPSP 2018)

Transient-based protection technique for future DC grids utilising travelling wave power

eISSN 2051-3305
Received on 3rd May 2018
Accepted on 23rd May 2018
E-First on 10th September 2018
doi: 10.1049/joe.2018.0186
www.ietdl.org

Monday Ikhide[1] ✉, Sarath Tennakoon[1], Alison Griffiths[1], Hengxu Ha[2], Sankara Subramanian[2], Andrzej Adamczyk[2]

[1]*Department of Engineering, Staffordshire University, College Road, Stoke-on-Trent, UK*
[2]*GE Power, Redhill Business Park, Stafford, UK*
✉ *E-mail: monday.ikhide@coventry.ac.uk*

Abstract: This study presents a novel time-domain protection technique for application to DC grids. The technique utilises the power developed by the forward and backward travelling waves produced by a fault to distinguish between internal and external faults. For an internal fault, the calculated travelling wave power must exceed a predetermined setting; otherwise the fault is external. The ratio between the forward travelling wave power and the backward travelling wave power provides a directional comparison. For a forward directional fault, this ratio is less than unity, whereas the ratio is greater than unity for reverse directional faults. To improve the sensitivity of the protection scheme for long-distance remote internal fault, a second element utilising the concavity of the forward travelling wave power is proposed. The proposed technique is time domain based and does not require complex mathematical burden; moreover, as such can be easily implemented since it will require fewer hardware resources. Simulations were carried out in power systems computer-aided design/electromagnetic transient simulations, and the results presented considering wider cases of fault scenarios including 500 Ω remote internal fault shows the suitability of the proposed scheme as all fault scenarios indicated were identified within 500 μs following the application of the fault.

1 Introduction

The availability of fast fault detection algorithms is a prerequisite for the secure and reliable operation of multi-terminal HVDC systems also termed DC grids [1–8]. This is because DC fault current rises rapidly due to the low inductance in DC systems compared with AC systems, thus reaching damaging levels in a few milliseconds [2]. Therefore, fault detection, discrimination and clearance in DC grids must be completed before the fault current reaches a damaging level to ensure that the faulty section is isolated quickly while maintaining the continuity of service delivery in the healthy section of the grid. However, a major issue is selectivity; as only the faulty section should be isolated in the event of a fault. The challenge is to realise this using single-ended measurements only, without information from the remote end relay(s) via a communication link. In the light of these constraints, transient-based protection techniques are ideal candidates for DC grid protection.

Transient-based protection techniques utilise the fault generated transient components to detect the occurrence of faults, thereby making it possible to detect the fault very quickly, and well before the steady state. The conventional current derivative ($\mathrm{d}i/\mathrm{d}t$) protection technique developed for DC traction systems, the voltage derivative protection technique ($\mathrm{d}v/\mathrm{d}t$) used in two-terminal HVDC systems, the polarity identification technique, as well as the travelling wave-based protection (TWBP) techniques, belong to the class of transient-based protection technique. However, there are some limitations in adopting them for the protection of DC grids. For example, the traditional $\mathrm{d}v/\mathrm{d}t$ developed for two-terminal HVDC systems cannot provide directional discrimination, whilst the $\mathrm{d}i/\mathrm{d}t$ techniques applicable to DC traction systems such as $\mathrm{d}i/\mathrm{d}t + \Delta T$ or $\mathrm{d}i/\mathrm{d}t + \Delta i$ [9] would require a long time window to provide discrimination, thereby incurring delays. Therefore, for DC grid protection, the initial $\mathrm{d}i/\mathrm{d}t$ must be accurately measured to guarantee the reliability of the protection scheme. The polarity identification technique would also require communication between the local and remote end relays and as such incur communication delays. In the same way, TWBP techniques relying on multiple reflections between the fault and relay terminals will also result in communication delay noting that the wave propagation delay time may be more than the time required to detect, discriminate and clear the fault. Furthermore, TWBP techniques relying on complex digital signal processing (DSP) techniques will involve computational burden and incur a delay, thus consuming hardware resources. Therefore, new TWBP techniques must be developed for DC grids application.

Several attempts have been made in the recent past to adopt the aforementioned principles or a combination of two or more to develop DC line protection scheme for application to DC grids [3–7], whereas more still needs to be done. The protection technique presented in this paper is based on a travelling wave propagation theory. The power developed by the forward and backward travelling waves following the occurrence of a fault is extracted for processing in order to determine whether a fault has occurred or not. For an internal fault, the calculated travelling wave power must exceed a predetermined setting; otherwise the fault is external. The ratio between the forward travelling wave power and the backward travelling wave power provides a directional comparison. For a forward directional fault, this ratio must be less than unity whereas it is greater than unity for a reverse directional fault (RDF). To improve the sensitivity of the protection scheme for long-distance remote internal faults, a second element utilising the concavity of the forward travelling wave power is also proposed.

2 Basic philosophy

Any fault on a transmission line will generate a travelling wave (Fig. 1), which travels back and forth between the fault and the relay terminals until they are damped and the post-fault steady-state conditions are attained [10].

As shown in Fig. 1, the assumed positive (or reference) direction of current flow in the relay is from the bus bar into the line. Therefore, v_{BA} and v_{BB} are backward voltage travelling waves (BVTWs) whilst v_{FA} and v_{FB} are forward VTWs (FVTWs) with respect to relays A and B, respectively. Now, considering fault F with respect to terminal A of Fig. 1, the following expressions can be written:

This is an open access article published by the IET under the Creative Commons Attribution License
(http://creativecommons.org/licenses/by/3.0/)

$$v_{FA}(x, t) = \frac{\Delta v_{DC}(x, t) + Z_C \Delta i_{DC}(x, t)}{2} \quad (1)$$

$$v_{BA}(x, t) = \frac{\Delta v_{DC}(x, t) - Z_C \Delta i_{DC}(x, t)}{2} \quad (2)$$

The power contained in the forward and backward travelling waves P_{FW} and P_{BW}, respectively, can also be expressed as

$$P_{FW}(t) = \frac{1}{Z_C} v_{FA}(t)^2 \quad (3)$$

$$P_{BW}(t) = -\frac{1}{Z_C} v_{BA}(t)^2 \quad (4)$$

Further simplifications result in

$$P_{FW}(t) = \frac{1}{4Z_C}(\Delta v_{DC}^2 + 2\Delta v_{DC}\Delta i_{DC}Z_C + \Delta i_{DC}^2 Z_C^2) \quad (5)$$

$$P_{BW}(t) = -\frac{1}{4Z_C}(\Delta v_{DC}^2 - 2\Delta v_{DC}\Delta i_{DC}Z_C + \Delta i_{DC}^2 Z_C^2) \quad (6)$$

Z_c is the surge impedance of the line and Δv_{DC}; Δi_{DC} is the superimposed components of the DC voltage and current.

3 Protection principle

Consider the schematic diagram shown in Fig. 2. The inductors L showed are representative of di/dt limiting inductors as per the HVDC circuit breaker or fault current limiters (FCLs) [3]. As shown, F_1 and F_3 are forward faults with respect to relay R_{12}, whereas F_2 is a reverse fault. However, F_1 is also an internal whilst F_2 and F_3 are external faults. Therefore, F_1 is a *forward internal fault* (*FIF*) and F_3 is a *forward external fault* (*FEF*). The goal is to operate the relay only for internal faults (F_1 as shown) and not operate for external faults (F_2 and F_3 as shown).

3.1 Forward and reverse faults

Considering Fig. 3*a*, when the BVTW from fault F_1 reaches the relay terminals (say terminal *A*), the first incident wave at R_{12} is v_{BA}, which is reflected to produce v_{FA}.

In practise, the reflected waves at a boundary have lower magnitude compared with the magnitude of the incident wave. Hence, v_{FA} is less than v_{BA} for a specified brief period following fault inception. Therefore

$$v_{FA} < v_{BA} \text{ or } \frac{v_{FA}}{v_{BA}} < 1$$

Therefore, from (1) to (6)

$$\frac{P_{FW}}{P_{BW}} < 1$$

Now considering Fig. 3*b*, and with a fault F_2 (a reverse fault with respect to relay R_{12}), the first wave seen by R_{12} is v_{FA}; which is now a forward voltage travelling wave with respect to R_{12}. A significant amount of time will, therefore, elapse before the arrival of v_{BA} at terminal A following a reflection at terminal B. Therefore, for fault F_2, the magnitude of v_{FA} is greater than v_{BA}, and we can write

$$v_{FA} > v_{BA} \text{ or } \frac{v_{FA}}{v_{BA}} > 1; \quad \frac{P_{FW}}{P_{BW}} > 1$$

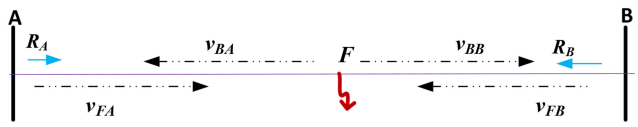

Fig. 1 *Travelling waves on a transmission line*

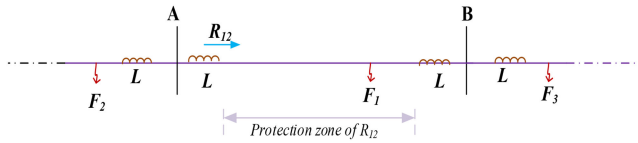

Fig. 2 *Transmission network showing arbitrary fault locations*

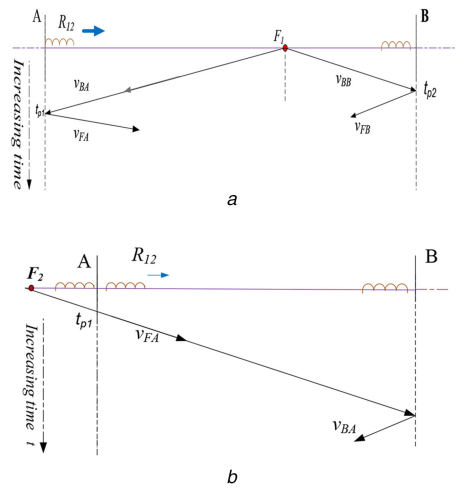

Fig. 3 *Conditions for forward and reverse faults*
(a) Forward directional fault, ***(b)*** reverse directional fault , t_p = propagation delay of the travelling wave

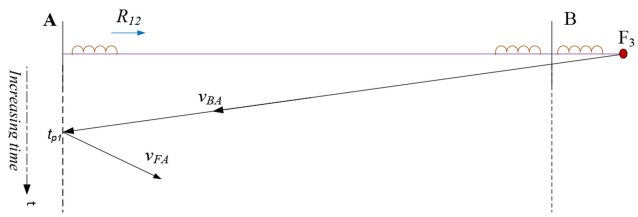

Fig. 4 *Conditions for internal and external faults*

Table 1 Conditions for internal fault

Condition	Type
$\frac{P_{FW}}{P_{BW}} < 1$	ratio check
$P_{FW} > P_{FW\,(set)}$	magnitude check 1
$P_{BW} > P_{BW\,(set)}$	magnitude check 2

P_{FW}/P_{BW} is the travelling wave power ratio P_r.

3.2 Forward internal and forward external faults

In Fig. 4, R_{12} sees a much attenuated BVTW and FVTW; hence, reduced magnitudes of P_{FW} and P_{BW} due to the discontinuity or boundary at terminal B.

This is largely due to the DC inductor located at each of the line ends, which provides attenuation to the high-frequency components resulting from an external fault. However, the attenuation of a travelling wave due to FIF such as F_1 in Fig. 3*a* is much smaller. This characteristic provides a method to discriminate between FIF and FEF. The general conditions for internal and external faults with respect to a local relay are summarised in Table 1.

This is an open access article published by the IET under the Creative Commons Attribution License (http://creativecommons.org/licenses/by/3.0/)

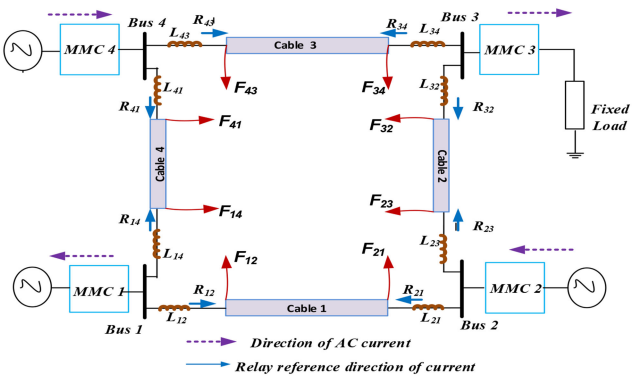

Fig. 5 *Four-terminal DC grid [11]*

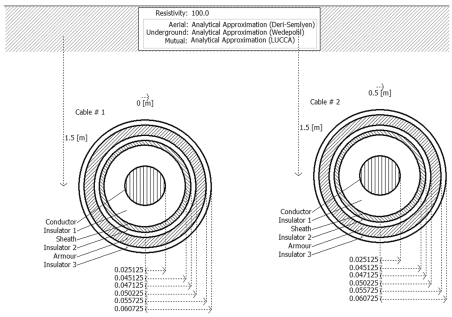

Fig. 6 *Cable configuration and geometry*

4 Validations

4.1 Test model

To validate the proposed protection technique, simulations were carried out as shown in Fig. 5. The test model consists of a four-terminal DC grid made available in power systems computer-aided design/electro-magnetic transient design and control [11]. However, some adjustments were made to the model to reflect the scenarios under consideration in this paper.

The network consists of four cable sections and four modular multi-level converters (MMCs) based on half-bridge submodule configuration. Details of the converter and AC parameters including the load parameter are given in Fig. 6, Tables 2 and 3. The cables are of frequency-dependent distributed parameter models, and as such the wave effects including attenuation, losses and the distortion have been accounted for (Fig. 6, Tables 2 and 3). All cable sections have a length of 200 km and all faults were assumed to be pole-ground faults and were applied at 2 s from the start of the simulation. All measurements were taken at the positive pole terminal of the DC cable. Air-cored inductors of 1 mH were placed at the DC cable ends to represent the inductive effects of HVDC breakers or FCLs [3]. These inductors also help to limit the di/dt during DC side short circuits.

4.2 Sampling frequency

As per international electrotechnical commission (IEC) guidelines for DC protection [8], the sampling frequency f_S used in this paper was 96 kHz. The measurement time window T_W or window length for the relay decision must be within a predetermined time frame following the detection of the transient. Since travelling waves damp quickly, typically <1 ms following the arrival of the first incident wave at the relay terminal, the window length T_W was assumed to be 500 µs in this paper. Generally, this is a matter of compromise and, therefore, could vary depending on the designer and grid configuration. The sampling period T_S is given by

$$T_S = \frac{1}{96\,\text{kHZ}} = 10.42\,\mu\text{s}$$

The total number of samples for relay decision N_T was also determined; thus

Table 2 Converter and AC side parameters

Item	Ratings
rated power of the converter	800 MVA
rated DC voltage of the converter	400 kV
converter arm inductance	29 mH
cell DC capacitor	10,000 µF
nominal frequency	50 Hz
transformer nominal voltage $_{(L\text{-}L)}$ RMS	380 kV
nominal voltage at voltage-source converter side $_{(L\text{-}L)}$ RMS	220 kV
leakage reactance of the transformer	0.18 pu
rated real power per phase of load	33 MW
rated reactive power per phase of load	0.0 MW
rated load voltage$_{(L\text{-}G)}$ rms	83.72 kV

Table 3 Conductor and insulation parameters

Items	Dimensions
resistivity of the core conductor	2.2×10^{-8} Ωm
resistivity of the first conducting layer	27.4×10^{-8} Ωm
resistivity of the second conducting layer	18.15×10^{-8} Ωm
outer radius of the core conductor	2.51×10^{-2} m
thickness of the first conducting layer	2×10^{-3} m
thickness of the second conducting layer	5.5×0^{-3} m
thickness of the first insulation layer	2×10^{-2} m
thickness of the second insulation layer	3.1×10^{-3} m
thickness of the third insulation layer	5×10^{-3} m
relative permittivity of all insulation layer	2.3
all relative permeability	1
ground resistivity	100 Ωm
length of cable	200 km

$$N_T = \frac{T_W}{T_S} = \frac{500\,\mu\text{s}}{10.42\,\mu\text{s}} = 48\,\text{samples}$$

Following the application of fault on the DC link, the DC voltages and currents, v_{DC} and i_{DC}, respectively, at the respective relay terminals were sampled based on three point moving average to obtain the average DC voltages and currents, v_{DC}(Avg) and i_{DC}(Avg), and thereafter the incremental quantities Δv_{DC} and Δi_{DC} were determined. Thus

$$\Delta v_{DC} = v_{DC}(\text{Avg}) - v_{DC}(\text{steady state}) \quad (7)$$

$$\Delta i_{DC} = i_{DC}(\text{Avg}) - i_{DC}(\text{steady state}) \quad (8)$$

Following this, P_{FW} and P_{BW} were calculated based on (5) and (6), respectively.

4.3 Simulation results and discussion

Considering Fig. 5, under steady-state condition, MMC1 and MMC3 operate as rectifiers and as such imports power from the AC side whilst MMC2 and MMC4 operate as inverters exporting power to the load and AC grid, respectively. The steady-state bus bar voltages and the respective relay currents are given in Table 4. Simulations were carried out considering the worst-case scenario for all local relays indicated in Fig. 5. Ideally, this is a high-resistance remote FIF versus a low-resistance FEF on an adjacent cable section as well as an RDF. For example, with respect to relay R_{12}, the worst-case fault scenario is arrived at by considering fault F_{21} with a fault resistance $R_f = 500\,\Omega$ against fault F_{23} and F_{14} with $R_f = 0.01\,\Omega$. The same scenario holds for the remaining relays

This is an open access article published by the IET under the Creative Commons Attribution License
(http://creativecommons.org/licenses/by/3.0/)

Table 4 Steady-state DC voltage and current

Relay	Steady-state DC voltage, kV [$V_{dc(ss)}$]	Steady-state DC current, kA [$i_{dc(ss)}$]
R_{12}	198.54	−1.032
R_{21}	200.81	1.037
R_{23}	200.87	0.198
R_{32}	200.46	−0.195
R_{34}	200.56	−0.051
R_{43}	200.72	0.059
R_{14}	200.64	0.897
R_{41}	198.64	0.899

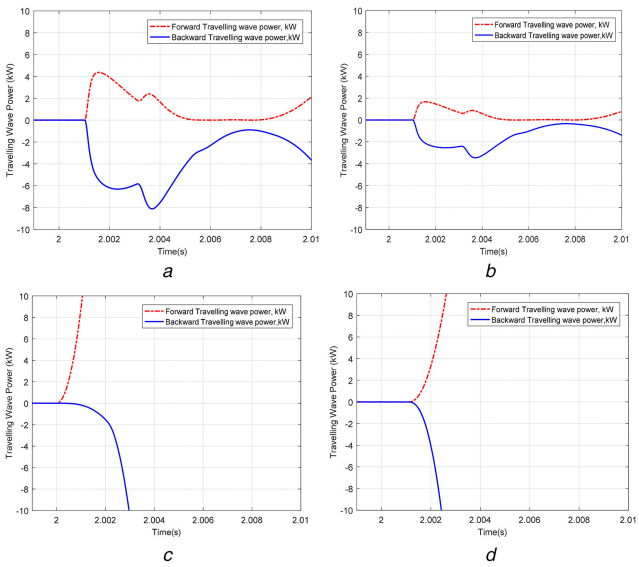

Fig. 7 *Simulation results considering internal and external faults*
(a) FIF; R_f=500 Ω, ***(b)*** FIF; R_f=300 Ω, ***(c)*** RDF; R_f=0.01 Ω, ***(d)*** FEF; R_f=0.01 Ω

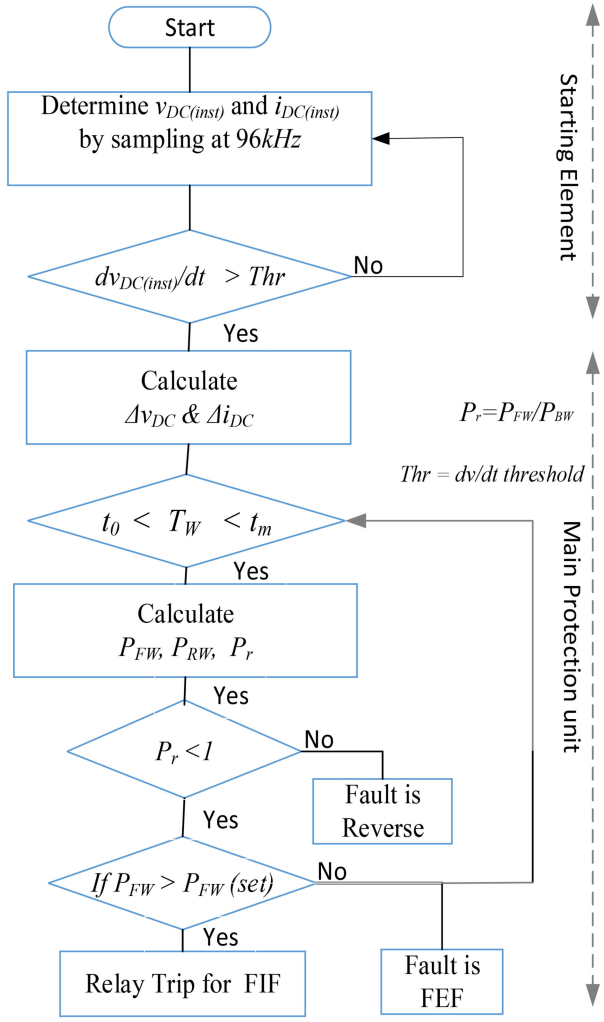

Fig. 8 *Flowchart of the proposed TWBP technique*

indicated as shown. However, due to limited space, only the plots obtained considering R_{12} are presented in this paper.

The calculated travelling wave power components (P_{FW} and P_{BW}) with respect to relay R_{12} considering faults F_{21}, F_{23} and F_{14} are presented in Fig. 7. As shown, under steady-state conditions, P_{FW} and P_{BW} are zero indicating that no travelling waves are present. However, at the instant of fault inception (after 2 s), travelling waves are generated and travel along the cables; moreover, as such P_{FW} and P_{BW} are developed by the travelling waves. Generally, a significant amount of time will elapse (depending on the distance between the relay terminal and the fault) until the travelling wave components arrive at the relay terminal. For example, the arrival time of the travelling waves at R_{12} due to fault F_{21} is 2.00102 s while that for F_{23} and F_{14} are 2.00112 and 2.0005 s, respectively. However, this is not a major issue because as far as the relay is concerned, the arrival time of the travelling wave is taken as t_0. This is usually determined by incorporating a starting element (such as dv/dt in this study). Now considering Fig. 7*a* (FIF; R_f = 500 Ω), the magnitude of P_{BW} recorded at the relay terminal during the first few milliseconds following the arrival of the first incident wave exceeds that of P_{FW} indicating that F_{21} is an FDF with respect to R_{12}. Therefore, the ratio P_{FW}/P_{BW} during the measurement period will be less than unity. The same also holds in Fig. 7*b* (FIF; R_f = 300 Ω), but with a reduced magnitude of the travelling wave components. This is consistent with the travelling wave theory as the magnitudes of the resulting travelling wave components are largely dependent on the fault resistance [12]. However, in Fig. 7*c* (RDF; R_f = 0.01 Ω), the magnitude of P_{FW} exceeds that of P_{BW} during the measurement period indicating that F_{14} is an RDF with respect to R_{12}, and, therefore, the ratio P_{FW}/P_{BW} will be greater than unity. These characteristics are consistent with the conditions established in Section 3 for directional discrimination.

It can be seen from Fig. 7*d* (FEF; R_f = 0.01 Ω) that though the calculated P_{BW} exceeds that of P_{FW} hence indicating an FDF; however, the calculated P_{FW} and P_{BW} for F_{21} significantly exceed that for F_{23}. This is because the high-frequency components of the fault generated transient components from F_{23} are attenuated at the boundary consisting of the bus bar 2, inductors L_{21} and L_{23}, respectively. This characteristic is consistent with that stipulated in Table 1 as per magnitude criteria and it provides discrimination between FIF and FEF. To guarantee the reliability of the protection scheme, the actual signals used for relay decision were taken during the first 500 µs following the detection of the transient. This corresponds to 48 samples as explained in Section 4.2. The flowchart is shown in Fig. 8. The calculated P_{FW} and P_{BW} considering all scenarios indicated in Fig. 5 are presented in Table 5. In all cases, and with respect to all local relays indicated, the magnitudes P_{FW} and P_{BW} for FIF for large fault resistance (R_f = 300 Ω, 500 Ω) exceed those of FEF with low fault resistances (R_f = 0.01 Ω). Furthermore, the travelling wave power ratio P_r is less than unity indicating that all fault scenarios indicated are forward faults with respect to the local relays. Generally, the conditions for FDF or RDF have been established in Fig. 7.

Still considering Table 5, a protection threshold of $P_{FW(set)}$ = 1.50 kW and $P_{BW(set)}$ = 1.80 kW will accurately and reliably discriminate between an FIF and FEF (Fig. 9). It can be seen from the expanded plot shown in Fig. 9*c* that though P_{FW} for RDF may exceed the protection setting of 1.50 kw, however, the relay will not operate as the ratio criteria and is not satisfied. Generally, a safety margin will be introduced to account for non-uniformity of the cable geometry and measurement errors. In practise, this will

This is an open access article published by the IET under the Creative Commons Attribution License
(http://creativecommons.org/licenses/by/3.0/)

Table 5 Calculated P_{FW} and P_{BW} based on Fig. 5

Local relay	Fault location	Fault type with respect to the local relay	Fault resistance, Ω	$\lvert P_{FW}\rvert$, kW	$\lvert P_{BW}\rvert$, kW	P_r
R_{12}	F_{21}	FIF	300	4.25	5.03	0.84
	F_{21}	FIF	500	1.52	1.82	0.81
	F_{23}	FEF	0.01	0.75	0.82	0.92
R_{21}	F_{12}	FIF	300	4.16	5.13	0.81
	F_{12}	FIF	500	1.61	1.97	0.82
	F_{14}	FEF	0.01	0.91	0.98	0.92
R_{23}	F_{32}	FIF	300	4.27	5.32	0.80
	F_{32}	FIF	500	1.65	2.04	0.81
	F_{34}	FEF	0.01	1.29	1.45	0.88
R_{32}	F_{23}	FIF	300	4.41	5.40	0.82
	F_{23}	FIF	500	1.71	2.10	0.81
	F_{21}	FEF	0.01	1.18	1.34	0.88
R_{34}	F_{43}	FIF	300	4.46	5.38	0.83
	F_{43}	FIF	500	1.74	2.09	0.83
	F_{41}	FEF	0.01	0.96	1.15	0.83
R_{43}	F_{34}	FIF	300	4.46	5.54	0.80
	F_{34}	FIF	500	1.76	2.18	0.81
	F_{32}	FEF	0.01	1.16	1.37	0.85
R_{41}	F_{14}	FIF	300	4.32	5.08	0.85
	F_{14}	FIF	500	1.78	2.17	0.82
	F_{12}	FEF	0.01	1.01	1.11	0.91
R_{14}	F_{41}	FIF	300	4.18	5.17	0.81
	F_{41}	FIF	500	1.71	2.09	0.82
	F_{43}	FEF	0.01	1.09	1.31	0.83

FIF: Forward internal fault; FEF: Forward external fault; $P_r = |P_{FW}|/|P_{BW}|$.

be a matter of comprise and will depend on the designer and grid configuration. Extensive simulations carried out revealed that the magnitudes of P_{FW} and P_{BW} for a pre-set time duration (500 µs in this paper) following the occurrence of fault decreases exponentially with increasing fault distance (Fig. 10). The significance of this plot is that it can be used to determine the relay settings for varying fault distances, thus a generic model can be developed, and the protection threshold determined off-site provided the cable parameters are known. However, this will involve extensive simulations and the use of a reliable curve fitting technique to avoid spurious relay trips.

4.4 Fault discriminative criteria utilising travelling wave power concavity

As shown in Fig. 11, care must be taken to ensure that measurements are taken before the travelling wave components damp out as the magnitude of P_{FW} or P_{BW} for low-resistance FEF may exceed that of high-resistance FIF. This can lead to spurious relay trips. To account for this, the wave shape of the calculated P_{FW} is proposed to provide discrimination between FIF and FEF.

The plots of P_{FW} and P_{BW} considering the fault scenarios indicated in Fig. 5 with respect to R_{12} considering 48 samples ($N_T = 48$) are shown in Figs. 12*a*–*d*. As shown, the coefficient of t^2 is negative in Figs. 12*a* and *b*, and hence the second derivative must be negative indicating a '*concave-downwards*' travelling wave components. However, in Figs. 12*c* and *d*, the travelling wave components show a '*concave-upwards*' characteristics, and therefore the second derivative of the function is positive, indicating an external fault. For an internal fault with respect to a local relay, the second derivate of the travelling wave power curve is negative, whereas it is positive for external faults. This phenomenon is likely to be attributed to the reflection and refraction characteristics at the boundary thus leading to 180° phase shift. Thus

$$\ldots\text{if}\quad \frac{d^2P_{FW}}{dt^2} < 0;\ \text{fault is internal}$$

$$\ldots\text{else if}\quad \frac{d^2P_{FW}}{dt^2} > 0;\ \text{fault is external}$$

4.5 Proposed back-up protection

For a back-up protection, the travelling wave power components at both the local and remote end relay terminals could be determined and a communication established via an optical fibre as shown in Fig. 13. The integrity of the communication system would, therefore, play a key role in adopting this principle.

Thus

$$\ldots\text{if}\ \frac{P_{FW_1}}{P_{BW_1}}\ \text{AND}\ \frac{P_{FW_2}}{P_{BW_2}} < 1;\ \text{fault is internal}$$

$$\text{else if}\ \frac{P_{FW_1}}{P_{BW_1}}\ \text{OR}\ \frac{P_{FW_2}}{P_{BW_2}} > 1;\ \text{fault is external}$$

where the subscripts 1 and 2 represent the travelling wave power components at local and remote end relays, respectively.

5 Conclusions

This paper presents some proposals for consideration in DC grid protection. The study focuses on the DC line fault detection algorithm; hence, the effect of the converter operation on the travelling wave components is outside the scope of this paper. The proposed protection principle utilises the power developed by the forward and backward travelling waves following the occurrence of the fault. The simulation results presented show the

This is an open access article published by the IET under the Creative Commons Attribution License
(http://creativecommons.org/licenses/by/3.0/)

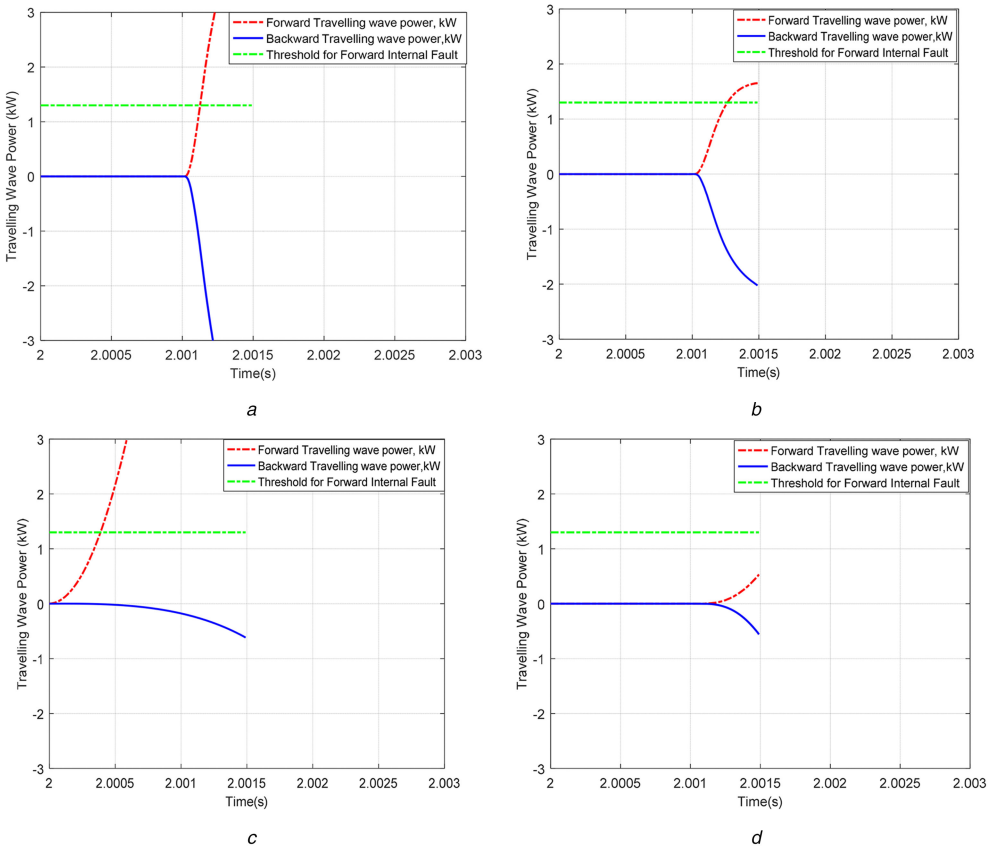

Fig. 9 *Expanded plot of Fig. 7*
(a) FIF; R_f=500 Ω, ***(b)*** FIF; R_f=300 Ω, ***(c)*** RDF; R_f=0.01 Ω, ***(d)*** FEF; R_f=0.01 Ω

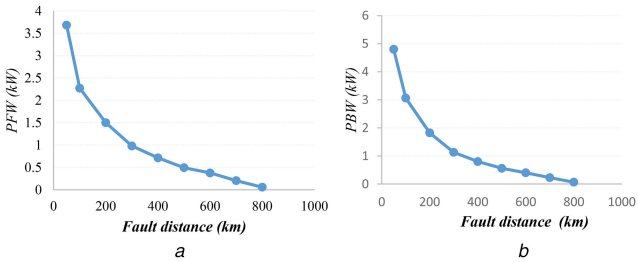

Fig. 10 *Variation of PFW and PBW with increasing fault distance*
(a) P_{FW}; R_f=500 Ω, ***(b)*** P_{BW}; R_f=500 Ω

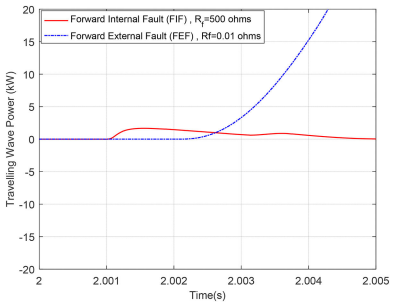

Fig. 11 *Comparison of high-resistance FIF versus low-resistance FEF*

effectiveness of the proposed principle in discriminating between internal and external faults. A key advantage of this technique is that it is non-unit based, hence no communication delays. Also, as it time domain based, it does not require complex computational/DSP techniques, which ultimately will result in less computational burden thus requiring minimal hardware resources and saving cost.

The practical application of the proposed technique is dependent on the availability of commercially available relays having the capability of sampling at 96 kHz or more. The study also assumes a pure relay signal as per proof-of-concept. However,

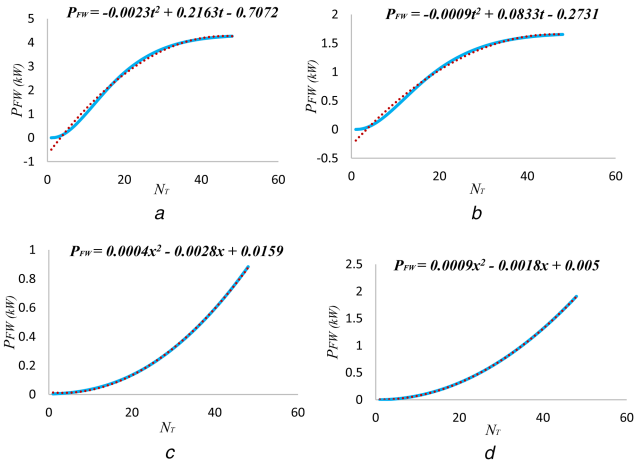

Fig. 12 *Concave-up versus concave-down fault discriminative criteria*
(a) P_{FW}: FIF; R_f=300 Ω, ***(b)*** P_{FW}: FIF; R_f=500 Ω, ***(c)*** P_{FW}: FEF; R_f=0.01 Ω, ***(d)*** P_{FW}: RDF; R_f=0.01 Ω

the effect of noise on the proposed protection technique shall be investigated in future work. For close-up faults where the effect of the overlapping travelling wave may predominate, the simple and traditional impedance-based protection principle would be an ideal candidate. The main contribution of this paper is to develop a protection scheme that will be sensitive to high-resistance and long-distance remote internal faults. The proposed protection technique will also find useful applications in low-voltage DC distribution systems.

6 Acknowledgments

Thanks are due to the management and staff of GE Grid Solutions, Stafford for providing financial support for this research project. Special thanks also go to Staffordshire University for providing the

This is an open access article published by the IET under the Creative Commons Attribution License
(http://creativecommons.org/licenses/by/3.0/)

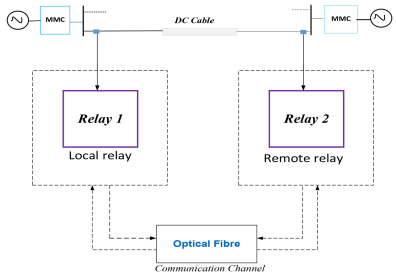

Fig. 13 *Proposed back-up protection scheme*

enabling environment to study for a research degree in the first instance.

7 References

[1] Jovcic, D., Hertem, D.V., Linden, K., *et al.*: 'Feasibility of DC transmission networks'. Second IEEE PES Int. Conf. Exhibition on Innovative Smart Grid Technology, Manchester, UK, December 2011, pp. 1–8

[2] Barker, C.D., Whitehouse, R.S.: 'An alternative approach to HVDC grid protection'. Tenth IET Int. Conf. AC and DC Power Transmission (ACDC 2012), Birmingham, UK, May 2012, pp. 1–6

[3] Sneath, J., Rajapakse, A.D.: 'Fault detection and interruption in an earthed HVDC grid using ROCOV and hybrid DC breakers', *IEEE Trans. Power Deliv.*, 2016, **31**, (3), pp. 973–981

[4] Adamczyk, A., Barker, C.D., Ha, H.H.: 'Fault detection and branch identification for HVDC grids'. 12th IET Int. Conf. Developments in Power System Protection (DPSP 2014), Copenhagen, Denmark, April 2014, pp. 1–6

[5] Dallas, I., Booth, C.C: 'Teleprotection in multi-terminal HVDC supergrids'. 12th IET Int. Conf. Developments in Power System Protection (DPSP 2014), Copenhagen, Denmark, April 2014, pp. 1–6

[6] Wang, J., Berggren, B., Linden, K., *et al.*: 'Multi-terminal DC system line protection requirement and high speed protection solutions'. CIGRE, Lund, Sweden, 2015, pp. 1–9

[7] Ikhide, M., Tennakoon, S.B., Alison, A.L., *et al.*: 'Fault detection in multi-terminal modular multilevel converter (MMC) based high voltage DC (HVDC) transmission system'. IEEE Conf. Universities Power Engineering Conf. (UPEC), Stoke-on-Trent, UK, 2015, pp. 1–6

[8] 'Implementing the protection and control of future HVDC grids, Think Grid'. Available at: http://www.think-grid.org/implementing-protection-and-control-future-hvdc-grids, accessed 2 May 2017

[9] Li, M.X., He, J.H., Bo, Z.Q., *et al.*: 'Simulation and algorithm development of protection scheme in DC traction systems'. IEEE Powertech Conf., Bucharest, Romania, 2009, pp. 1–6

[10] Crossley, P.A., McLaren, P.G.: 'Travelling wave based distance protection', *IEEE Trans. Power Appl. Syst.* 1983, **PAS-102**, (9), pp. 2971–2983

[11] Manitoba HVDC Research: 'Four Terminal DC test Grid', 2014. Available at: https://hvdc.ca/

[12] Christopoulos, C., Thomas, D.W.P., Wright, A.: 'Scheme, based on travelling-waves, for the protection of major transmission lines', *IEE Proc.*, 1998, **135**, (1), pp. 63–73

This is an open access article published by the IET under the Creative Commons Attribution License
(http://creativecommons.org/licenses/by/3.0/)